Atmos. Chem. Phys. Discuss., doi:10.5194/acp-2016-581, 2016
Manuscript under review for journal Atmos. Chem. Phys.
Published: 1 August 2016


Atmospheric Chemistry and Physics
Discussions

# Integrated studies of a regional ozone pollution synthetically affected by subtropical high and typhoon system in the Yangtze River Delta region, China

**Lei Shu[1], Min Xie[1*], Tijian Wang[1,2*], Pulong Chen[1], Yong Han[1], Shu Li[1], Bingliang Zhuang[1], Mengmeng Li[1], Da Gao[1]**

[1]School of Atmospheric Sciences, Nanjing University, Nanjing, China

[2]CMA-NJU Joint Laboratory for Climate Prediction Studies, Institute for Climate and Global Change Research, School of Atmospheric Sciences, Nanjing University, Nanjing, China

--------------------------------------------------------------------------------------------------

∗Corresponding author, +86-25-89685302

E-mail address: minxie@nju.edu.cn, tjwang@nju.edu.cn

**Abstract**: Severe high ozone ($O_3$) episodes usually have close relations to synoptic systems. A regional continuous $O_3$ pollution episode is detected over the Yangtze River Delta (YRD) region in China during August 7-12, 2013, in which the $O_3$ concentrations in more than half of the cities exceeding the national air quality standard. The maximum hourly concentration of $O_3$ reaches 167.1 ppb. By means of the observational analysis and the WRF/CMAQ numerical simulation, the characteristics and the essential impact factors of the typical regional $O_3$ pollution is integratedly investigated. The observational analysis shows that the atmospheric subsidence dominated by Western Pacific subtropical high plays a crucial role in the formation of high-level $O_3$. The favorable weather conditions, such as extremely high temperature, low relative humidity and weak wind speed, caused by the abnormal strong subtropical high are responsible for the trapping and the chemical production of $O_3$ in the boundary layer. In addition, when the YRD cities at the front of Typhoon Utor, the periphery circulation of typhoon system can enhance the downward airflows and cause worse air pollution. But when the typhoon system weakens the subtropical high, the prevailing southeasterly surface wind leads to the mitigation of the $O_3$ pollution. The Integrated Process Rate (IPR) analysis incorporated in CMAQ is applied to further illustrate the combined influence of subtropical high and typhoon system in this $O_3$ episode. The results show that the vertical diffusion (VDIF) and the gas-phase chemistry (CHEM) are two major contributors to $O_3$

formation. During the episode, the contributions of VDIF and CHEM to $O_3$ maintain the high values over 10 ppb/h in Shanghai, Hangzhou, and Nanjing. On August 10-11, the cities close to the sea are apparently affected by the typhoon system, with the contribution of VDIF increasing to 28.45 ppb/h in Shanghai and 19.76 ppb/h in Hangzhou. When the YRD region is under the control of the typhoon system, the contribution values of all individual processes decrease to a low level in all cities. These results provide an insight for the $O_3$ pollution synthetically impacted by the Western Pacific subtropical high and the tropical cyclone system.

**Keyword**: Ozone; subtropical high; typhoon; the Yangtze River Delta region; heat wave

## 1. Introduction

Ground-level ozone ($O_3$) is a secondary air pollutant generated by a series of complicated photochemical reactions involving nitrogen oxides ($NO_x$) and hydrocarbons (HC) (Crutzen, 1973; Sillman, 1999; Jenkin et al., 2000; Wang et al., 2006b; Xie et al., 2014; 2016b). Severe $O_3$ pollution events usually occur in the presence of sunlight and under favorable meteorological conditions, with the abundance of $O_3$ precursors ($NO_x$ and HC) (Wang et al., 2006b). These $O_3$ pollutions in troposphere can deteriorate the air quality, and thereby cause adverse effects on human health and vegetation (Feng et al., 2003; Fann and Risley, 2013; Landry et al., 2013). Consequently, the formation mechanism and the integrated prevention of $O_3$ pollution are of great concern in many megacities all over the world (Xie et al., 2016b).

Over the past decades, along with the rapid industrial and economic development, many areas in China have been suffering from high levels of $O_3$ pollution. Especially in the most economically vibrant and densely populated areas, such as the Yangtze River Delta (YRD) region, the Pearl River Delta (PRD) region, and the Beijing-Tianjin-Hebei (BTH) area, the severe $O_3$ pollution episode has frequently occurred (Lam et al., 2005; Wang et al., 2006b; An et al., 2007; Chan and Yao, 2008; Duan et al., 2008; Jiang et al., 2008; Zhang et al., 2008; Guo et al., 2009; Shao et al., 2009; Ma et al., 2012) , and the background air pollutant concentrations have steadily increased (Chan and Yao, 2008; Zhang et al., 2008; Tang et al., 2009; Wang et al., 2009a; Ma et al., 2012; Liu et al., 2013). Many studies on the $O_3$ pollution, including satellite data analyses, field experiments, and model simulations, have been carried out over China in order to investigate the temporal and spatial characteristics of surface photochemical pollutions (Lu and Wang, 2006;

Wang et al., 2006a; Tu et al., 2007; Zhang et al., 2007; 2008; Geng et al., 2008; Tang et al., 2008; 2009; Chen et al., 2009; Han et al., 2011; Ding et al., 2013; Xie et al., 2016b), nonlinear photochemistry of $O_3$ and its precursors (Lam et al., 2005; Ran et al., 2009; Liu et al., 2010; Li et al., 2011; Xie et al., 2014), interactions between $O_3$ and aerosols (Lou et al., 2014; Shi et al., 2015), the effects of urbanization on $O_3$ formation (Wang et al., 2007; 2009b; Liao et al., 2015; Li et al., 2016; Xie et al., 2016a; Zhu et al., 2016), and other essential impact factors (Jiang et al., 2012; Li et al., 2012; Wei et al., 2012; Liu et al., 2013; Gao et al., 2016).

The Yangtze River Delta (YRD) region is a highly developed area of urbanization and industrialization. With the accelerated economic development and remarkable increase in energy consumption, the photochemical smog with high level of $O_3$ concentration is becoming more and more prominent and frequent, tending to present conspicuous regional characteristics (Chan and Yao, 2008; Ma et al., 2012; Li et al., 2012). Being located on the southeastern coast of China, YRD features a typical subtropical monsoon climate and is strongly affected by the Western Pacific subtropical high in summer. So, high $O_3$ concentrations are usually observed in late spring and summer by in-situ monitoring (Ding et al., 2013; Xie et al., 2016b). Severe high $O_3$ episodes usually have close relations to synoptic systems (Huang et al., 2005; 2006; Wang et al, 2006b; Jiang et al., 2008; Cheng et al., 2014; Hung and Lo, 2015). Horizontal and vertical transport processes from upwind $O_3$-rich air masses as well as poor atmospheric diffusion conditions can lead to the accumulation of surface $O_3$ concentrations and aggravating the photochemical pollution (Wang et al., 2006b). In previous studies on high $O_3$ pollution in the YRD region, some researchers have discussed this issue. For example, Jiang et al. (2012) investigated the spring $O_3$ formation over East China, and suggested that $O_3$ concentrations over the YRD region were transported and diffused from surrounding areas. Li et al. (2014) presented quantitative analysis on atmospheric processes affecting $O_3$ concentrations in the typical YRD cities during a summertime regional high $O_3$ episode, and found that the maximum concentration of photochemical pollutants was usually related with the process of transportation. Gao et al. (2016) evaluated the $O_3$ concentration during a frequent shifting wind period, and revealed that vertical mixing played an important positive role in the formation of surface $O_3$. However, these investigations only focused on the $O_3$ formation mechanism for one megacity (such as Shanghai, Nanjing and Hangzhou, etc.) or just a single station. Up to now, studies on the process analysis of high ozone episodes over the

Atmos. Chem. Phys. Discuss., doi:10.5194/acp-2016-581, 2016
Manuscript under review for journal Atmos. Chem. Phys.
Published: 1 August 2016


YRD are quite limited (Li et al., 2012). So, more studies should pay attention to the typical weather systems and the exact formation mechanism of the regional $O_3$ pollution in this region.

During August 7-12 2013, there is a typical regional $O_3$ pollution episode in the YRD region, which may be combinedly influenced by the Western Pacific subtropical high and Typhoon Utor. To fill the knowledge gap and better understand the important factors impacting $O_3$ formation from the regional scale, we perform an observational analysis to identify the temporal and spatial characteristics of the episode. With the aid of the WRF/CMAQ as well as the Integrated Process Rate analysis (IPR) coupled within CMAQ, numerical simulations are conducted to provide qualitative and quantitative analysis on the contributions of individual atmospheric processes. The results may be a great help for the prediction and the prevention of high $O_3$ pollution events. In this paper, the brief description of observational data and model configurations are shown in Section 2. The detailed observational analysis of air quality and meteorological conditions are given in Section 3. The evaluation of model performance and the formation mechanism of $O_3$ explored by IPR technique are presented in Section 4. In the end, a summary of main findings is given in Section 5.

## 2. Methodology

### 2.1 Observed meteorological and chemical data

The weather charts and the observed surface meteorological records are used to analyze the synoptic systems during the episode in August 2013, as well as to evaluate the model results of meteorological factors. The weather charts for East Asia are accessible from Korea Meteorological Administration. The hourly meteorological data at the observation sites of SH (31.40°N,121.46°E) located in Shanghai, HZ (30.23°N, 120.16°E) in Hangzhou, and NJ (32.00°N, 118.80°E) in Nanjing can be obtained from the University of Wyoming, where 2-m air temperature, 2-m relative humidity, 10-m wind speed and10-m wind direction are available.

The air quality observational data are used to identify the regional characteristics of the $O_3$ episode and to validate the model performance for air pollutants. Fifteen cities are selected as the representative research objects to better reflect the status of $O_3$ pollution over the YRD region. The locations of these cities are shown in Fig. 1b, which contains Shanghai, 8 cities in Jiangsu province (Changzhou, Nanjing, Nantong, Suzhou, Taizhou, Wuxi, Yangzhou, and Zhenjiang), and

Atmos. Chem. Phys. Discuss., doi:10.5194/acp-2016-581, 2016
Manuscript under review for journal Atmos. Chem. Phys.
Published: 1 August 2016


6 cities in Zhejiang province (Hangzhou, Huzhou, Jiaxing, Ningbo, Shaoxing, and Zhoushan). The in-situ monitoring data for the hourly concentrations of $O_3$, CO, $NO_2$, $SO_2$, $PM_{2.5}$ and $PM_{10}$ can be acquired from National Environmental Monitoring Center (NEMC). The assurance/quality control (QA/QC) procedures for monitoring strictly follow the national standards (State Environmental Protection Administration of China, 2006). The hourly pollutant concentration for a city is calculated as the average of the pollutant concentrations from several national monitoring sites in that city, which can better characterize the pollution level of the city. In order to identify invalid or lacking data, a checking procedure for these data is performed following the work of Chiqueto and Silva (2010). Finally, only less than 0.2% of the primary data are ignored in the calculation.

### 2.2 Model description and configurations

WRF/CMAQ, which consists of the Weather Research and Forecasting (WRF) model version 3.4.1 and the Community Multi-scale Air Quality (CMAQ) Model version 4.7.1, is applied to simulate the high $O_3$ episode over the YRD region in August 2013. WRF is a new generation of meso-scale weather forecast model and assimilation system developed at the National Center for Atmospheric Research (NCAR). Numerous applications have proven that it shows a good performance in all kinds of weather forecasts and has broad application prospects in China (Jiang et al., 2008; 2012; Wang et al., 2009b; Liu et al., 2013; Xie et al., 2014; 2016a; Liao et al., 2014; 2015; Li et al., 2016; Zhu et al., 2016). WRF provides off-line meteorological fields as the input for the chemical transport model CMAQ. The CMAQ modeling system is a third generation of regional air quality model developed by the Environmental Protection Agency of USA (USEPA). A set of up-to-date compatible modules and control equations for the atmosphere is incorporated in the model, which can fully consider atmospheric complicated physical processes, chemical processes and the relative contribution of different species (Byun and Schere, 2006; Foley et al., 2010). CMAQ has been widely applied in China and proven to be a reliable tool in simulating air quality from city scale to meso scale (Li et al., 2012; Wei et al., 2012; Liu et al., 2013; Zhu et al., 2016).

The simulation run is conducted from 08:00 (LST) on August 2nd to 08:00 (LST) on August 16th 2013, in which the first 48 h is taken as the spin-up time. Three one-way nested domains are used in WRF with a Lambert Conformal map projection. The domain setting is shown in Fig.1. The outermost domain (domain 1, d01) covers the most areas of East Asia and South Asia, with

Atmos. Chem. Phys. Discuss., doi:10.5194/acp-2016-581, 2016
Manuscript under review for journal Atmos. Chem. Phys.
Published: 1 August 2016


the horizontal grids of 88×75 and the grid spacing of 81km. The nested domain d02 covers the southeastern part of China, with the horizontal grids of 85×70 and the grid spacing of 27km. The finest domain (domain 3, d03) covers the core areas of the YRD region, with the grid system of 70×64 and the resolution of 9km. For all domains, there are 23 vertical sigma layers from the surface to the top pressure of 100hPa, with about 10 layers in the PBL. The detailed configuration options for the dynamic parameterization in WRF are summarized in Table 1. Additionally, the SLAB scheme that does not consider urban canopy parameters is adopted to model the urban effect. In order to reflect the rapid urban expansion in the YRD region, the default USGS land-use archives are updated by adding the present urban land-use conditions from 500-m Moderate Resolution Imaging Spectroradiometer (MODIS) data, based on the work of Liao et al. (2014; 2015). The initial meteorological fields and boundary conditions are from NCEP FNL global reanalysis data with $1^{o}\times1^{o}$ resolution. The boundary conditions are forced every 6 h.

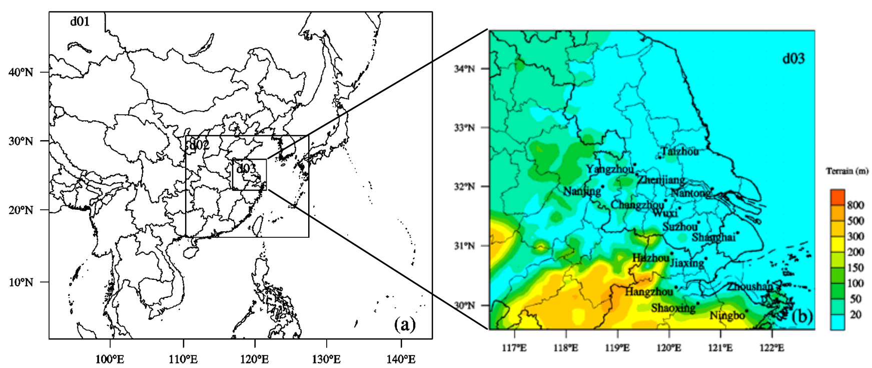


**Fig. 1. Domain settings, include (a) the three nested modeling domains and (b) the nested domain 3 (d03) with the terrain elevations and the locations of 15 main cities in the YRD region.**

**Table 1. The grid settings and the physical options for WRF in this study.**

| Items | Options |
|---|---|
| Dimensions(x, y) | (88, 75), (85, 70), (70, 64) |
| Grid spacing (km) | 81, 27 ,9 |
| Microphysics | WRF Single-Moment 5-class scheme (Hong et al., 2004) |
| Longwave Radiation | RRTM scheme (Mlawer et al., 1997) |

| | |
|---|---|
| Shortwave Radiation | Goddard scheme (Kim and Wang, 2011) |
| Surface layer | Moni-Obukhov scheme (Monin and Obukhov, 1954) |
| Land-surface layer | Noah Land Surface Model (Chen and Dudhia, 2001) |
| Planetary Boundary layer | YSU scheme (Hong et al., 2006) |
| Cumulus Parameterization | Grell-Devenyi ensemble scheme (Grell and Devenyi, 2002) |

With respect to the air quality model, CMAQ uses the same vertical levels and the similar three nested domains as those adopted in the meteorological simulation, whereas the CMAQ domains are one grid smaller than the WRF domains. The Meteorology Chemistry Interface Processor (MCIP) is used to convert WRF outputs to the input meteorological files needed by CMAQ. The Carbon Bond 05 chemical mechanism (CB05) (Yarwood et al., 2005) is chosen for gas-phase chemistry, and the 4rd generation CMAQ aerosol module (Byun and Schere, 2006) is adopted for aerosol chemistry. The initial and outmost boundary conditions are obtained from the Model for Ozone and Related Chemical Tracers version 4 (MOZART-4) (Emmons et al., 2010), while those for the two nested inner domains are extracted from the immediate concentration files of their parent domains. The anthropogenic emissions are mainly from the 2012-year Multi-resolution Emission Inventory for China (MEIC) with 0.25°× 0.25° resolution, which is re-projected for the grids of China in both domains. For the grids outside of China, the inventory developed for the Intercontinental Chemical Transport Experiment-Phase B (INTEX-B) by Zhang et al. (2009) is used. The natural $O_3$ precursor emissions are calculated by the natural emission model developed by Xie et al. (2007; 2009; 2014), including NO from soil, VOCs from vegetations, and $CH_4$ from rice paddies and terrestrial plants. The biomass burning emissions are acquired from the work of Xie et al. (2014; 2016a).

**2.3 Integrated Process Rate (IPR) analysis method**

The CMAQ modeling system contains process analysis module (PROCAN), which consists of the Integrated Process Rate (IPR) analysis and the Integrated Reaction Rate (IRR) analysis (Byun and Schere, 2006). IPR has the capability of calculating the hourly contributions of individual physical processes and the net effect of chemical reaction compared to the overall concentrations, and thereby can determine the quantitative contribution of each process in a specific grid cell. The atmospheric processes taken into consideration in IPR include the horizontal advection (HADV), the vertical advection (ZADV), the horizontal diffusion (HDIF),

Atmos. Chem. Phys. Discuss., doi:10.5194/acp-2016-581, 2016
Manuscript under review for journal Atmos. Chem. Phys.
Published: 1 August 2016

Atmospheric Chemistry and Physics
Discussions

the vertical diffusion (VDIF), the emissions (EMIS), the dry deposition (DDEP), the cloud processes with the aqueous chemistry (CLDS), the aerosol processes (AERO) and the gas-phase chemistry (CHEM). The IPR analysis has been widely applied to investigate the regional photochemical pollutions, and proven to be an effective tool to show the relative importance of every process and provide a fundamental interpretation (Goncalves et al., 2009; Li et al., 2012; Liu et al., 2013; Zhu et al., 2016).

In this paper, the period during August 4-15 is selected for the IPR analysis. With the aid of IPR, we assess the roles of the individual physical and chemical processes involved in $O_3$ formation over the YRD region, and further present those in the typical cities such as Shanghai, Nanjing and Hangzhou. Shanghai is the most populous city in China and Asia, as well as a global financial and transportation center. Locating to the northwest of Shanghai, Nanjing is the capital of Jiangsu Province and the second largest commercial center in East China. Hangzhou is the capital of Zhejiang Province and located to the southwest of Shanghai. These cities are all highly urbanized and industrialized, and suffer from severe $O_3$ pollution.

**2.4 Evaluation method**

Meteorological and air quality observation data are used to validate the reliability of simulation in this study. Comparisons of the modeling results in the finest domain (d03) with the hourly observation data are performed in Shanghai (31.40°N,121.46°E), Hangzhou (30.23°N, 120.16°E) and Nanjing(32.00°N, 118.80°E) for 2-m air temperature, 2-m relative humidity, surface $O_3$ and surface $NO_2$. Additionally, the modeling results and observations for the surface hourly $O_3$ concentrations in Wuxi (31.62°N, 120.27°E) is compared as well. The correlation coefficient (R), the normalized mean bias (NMB) and the root-mean-square error (RMSE) are used to evaluate the model performance. These statistic values are calculated as follows:

$$R = \frac{\sum_{i=1}^{N}(S_i - \bar{S})(O_i - \bar{O})}{\sqrt{\sum_{i=1}^{N}(S_i - \bar{S})^2}\sqrt{\sum_{i=1}^{N}(O_i - \bar{O})}} \quad (1)$$

$$NMB = \frac{\sum_{i=1}^{N}(S_i - O_i)}{\sum_{i=1}^{N}O_i} \times 100\% \quad (2)$$

$$RMSE = [\frac{1}{N}\sum_{i=1}^{N}(S_i - O_i)^2]^{\frac{1}{2}} \quad (3)$$

Atmos. Chem. Phys. Discuss., doi:10.5194/acp-2016-581, 2016
Manuscript under review for journal Atmos. Chem. Phys.
Published: 1 August 2016


Where $S_i$ represents the simulated value and $O_i$ represents the observed value. $N$ means the total number of valid data. Generally, the model performance is acceptable if the values of NMB and RMSE are close to 0 and that of R is close to 1.

## 3. Characteristics of the continuous ozone episode

### 3.1 Basic characteristic of the regional ozone episode in August 2013

Fig. 2 shows the temporal variation of the hourly $O_3$ concentrations observed by in-situ monitoring in 15 typical cities over the YRD region from 00:00 (UTC) 4 August to 23:00 (UTC) 15 August in 2013. Obviously, from August 7 to August 12, high $O_3$ concentrations over 93.5 ppb (approximately equal to the national air quality standard of 200 μg/m$^3$ for the hourly $O_3$ concentration) have been frequently recorded in 13 cities, which means most cities over the YRD region exceed the national air quality standard. So, this high $O_3$ pollution episode is a typical regional $O_3$ pollution episode that can affect the people and the ecosystem in a large area. Table 2 presents the highest and the average concentrations of $O_3$, as well as its precursors ($NO_2$ and CO), observed in these 15 cities during August 7- 12 2013. The highest hourly $O_3$ concentration occurs in Nantong with the value of 167.1 ppb, which is nearly 2 times of the national air quality standard, followed by 166.1 and 162.4 ppb in Changzhou and Jiaxing, respectively. It seems that $O_3$ concentrations are higher in the cities around Shanghai, where the concentrations of $O_3$ precursors (shown in Table 2) and the water vapor are more adequate as well. High concentrations of $O_3$ and its precursors imply that there may be stronger photochemical reactions in these cities.

Atmos. Chem. Phys. Discuss., doi:10.5194/acp-2016-581, 2016
Manuscript under review for journal Atmos. Chem. Phys.
Published: 1 August 2016


Atmospheric Chemistry and Physics
Discussions
Open Access

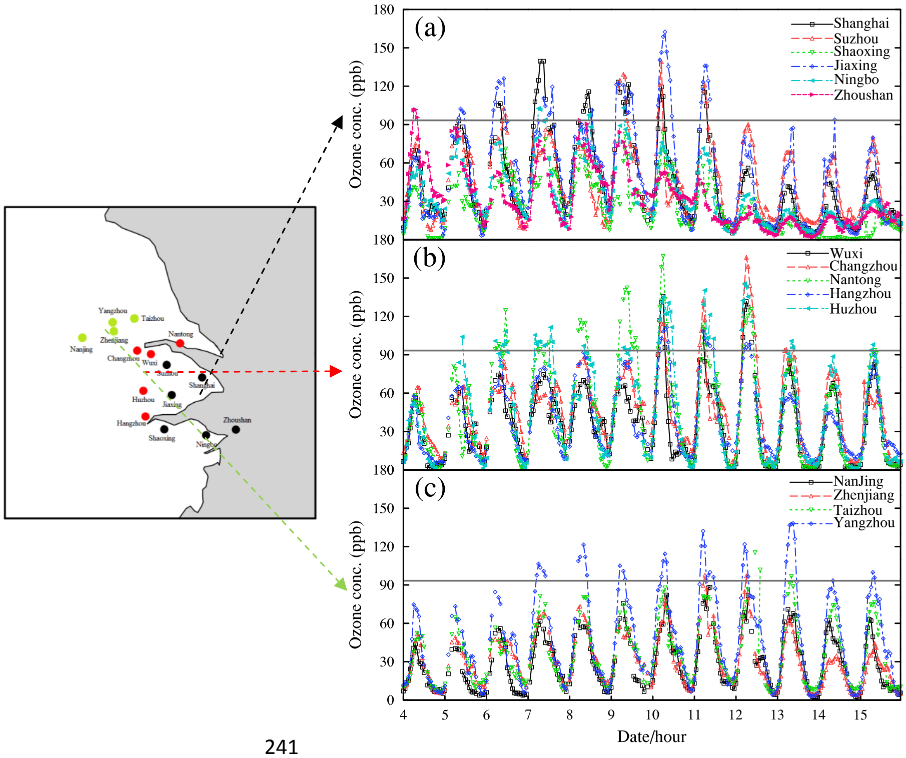


**Fig. 2. The time series of the observed $O_3$ concentrations in 15 typical cities from4 to 15 August 2013 over the YRD region, which can be divided into three areas: (a) the Southeast Coast Region (SCR), including Shanghai, Suzhou, Shaoxing, Jiaxing, Ningbo, and Zhoushan; (b) the Central Inland Region (CIR), including Wuxi, Changzhou, Nantong, Hangzhou, and Huzhou; (c) the Northwest Inland Region (NIR), including Nanjing, Zhenjiang, Taizhou and Yangzhou. The gray solid lines in (a), (b), and (c) represent the national standard for the hourly $O_3$ concentration, which is 200 μg/m$^3$.**

**Table 2. The maximum and average concentrations of $O_3$, $NO_2$, and CO observed in 15 cities (ppb)**

| Sites | | $O_3$ | | $NO_2$ | | CO | |
|---|---|---|---|---|---|---|---|
| | | Max | Mean | Max | Mean | Max | Mean |
| Southeast Coast Region (CSR) | Shanghai | 139.5 | 55.1 | 35.1 | 15.6 | 1184.0 | 605.5 |
| | Suzhou | 139.1 | 50.9 | 50.6 | 19.7 | 904.0 | 567.2 |
| | Jiaxing | 162.4 | 61.1 | 52.1 | 17.1 | 1128.0 | 671.6 |
| | Ningbo | 113.4 | 41.9 | 31.2 | 12.4 | 784.0 | 566.3 |
| | Shaoxing | 82.6 | 31.9 | 27.8 | 12.7 | 880.0 | 635.9 |
| | Zhoushan | 93.6 | 35.5 | 27.3 | 7.8 | 680.0 | 460.6 |
| Central Inland Region | Hangzhou | 111.5 | 48.6 | 30.2 | 16.7 | 712.0 | 472.1 |
| | Huzhou | 145.6 | 57.2 | 43.8 | 20.8 | 1040.0 | 661.3 |
| | Wuxi | 135.8 | 43.2 | 39.9 | 18.8 | 1824.0 | 785.3 |

| | | | | | | | |
|---|---|---|---|---|---|---|---|
| (CIR) | Changzhou | 166.1 | 55.7 | 58.4 | 24.5 | 1880.0 | 719.0 |
| | Nantong | 167.1 | 56.0 | 48.2 | 20.9 | 1224.0 | 655.4 |
| Northwest | Nanjing | 88.2 | 34.1 | 41.4 | 21.9 | 1640.0 | 813.9 |
| Inland | Yangzhou | 132.1 | 54.1 | 36.0 | 17.1 | 1568.0 | 710.1 |
| Region | Zhenjiang | 97.5 | 37.7 | 38.5 | 20.1 | 1752.0 | 963.0 |
| (NIR) | Taizhou | 115.3 | 40.5 | 18.5 | 7.7 | 1640.0 | 1094.0 |

According to the temporal variation characteristics of $O_3$ illustrated in Fig. 2, the abovementioned 15 typical YRD cities can be classified into three categories: (1) the cities in the Southeast Coastal Region (SCR), including Shanghai, Suzhou, Jiaxing, Ningbo, Shaoxing, and Zhoushan; (2) the cities in the Central Inland Region (CIR), including Hangzhou, Huzhou, Wuxi, Changzhou, and Nantong; and (3) the cities in the Northwestern Inland Region (NIR), including Nanjing, Yangzhou, Zhenjiang, and Taizhou. The classification is primarily on basis of the observational facts that the maximum $O_3$ concentrations occur on August 10-11, 12, and 13, and begin to synchronously decrease on August 12, 13 and 14 in SCR, CIR and NIR, respectively. As shown in Fig. 2, in the Southeast Coastal Region (SCR), Zhoushan firstly exceeds the national $O_3$ standard on August 4th, followed by Jiaxing, Shanghai, Suzhou and Ningbo. The peak hourly $O_3$ concentration of SCR occurs in Jiaxing on August 10 with the value up to 162.4 ppb. In the Central Inland Region (CIR), Huzhou is the first city exceeding the national $O_3$ standard, followed by the order of Nantong, Changzhou, Wuxi and Hangzhou. The high-level $O_3$ pollution in Huzhou lasts from August 5th to 13th. In Nantong and Changzhou, the maximum hourly $O_3$ concentration reaches 167.1 ppb on August 10 and 166.1 ppb on August 12, respectively. As for the Northwest Inland Region (NIR), Yangzhou, Zhenjiang and Taizhou successively exceed the national $O_3$ standard. It is also noteworthy that the date when $O_3$ concentration exceed the national air quality standard in coastal region is ahead of that in inland regions, so is the date of $O_3$ decrease. The different time of the $O_3$ decrease in different regions might be related to the strong southeast wind in accordance with the movement of Typhoon Utor, which is discussed in Sect. 3.2 in detail.

In general, for each city, there is a remarkable continuous growth in $O_3$ concentrations before the $O_3$ episode, followed by the lasting heavy $O_3$ pollution period. Though the $O_3$ concentrations in Shaoxing and Nanjing meet the national $O_3$ standard, their time series still show the similar tendency for the other cities in the same region. The excessive level of $O_3$ occurring in Huzhou,

Atmos. Chem. Phys. Discuss., doi:10.5194/acp-2016-581, 2016
Manuscript under review for journal Atmos. Chem. Phys.
Published: 1 August 2016


Atmospheric Chemistry and Physics Discussions

Jiaxing, Nantong, Yangzhou and Shanghai lasts for more than six consecutive days, reflecting the regional continuous characteristics of this $O_3$ pollution episode. As for $NO_2$ and CO, their average concentrations in the YRD region during the $O_3$ episode show the variation range of approximately 7.7~24.5 and 460.0~1094.0 ppb, respectively, indicating the heterogeneity of the spatial emission distribution of $O_3$ precursors. Besides, the relative high hourly concentrations of $NO_2$ show good agreements with those of $O_3$, implying it is one of the important $O_3$ precursor.

**3.2 Meteorological condition and its effect**

Favorable weather conditions have large impacts on the formation of severe $O_3$ pollution (Huang et al., 2005; 2006; Wang et al, 2006b; Jiang et al., 2008; Cheng et al., 2014; Hung and Lo, 2015). High-level $O_3$ episodes often take place in hot seasons, when the meteorological conditions with high temperature and strong solar radiation are beneficial to the photochemical reactions of $O_3$ (Lam et al., 2005). Fig. 3 shows the variations of the surface meteorological parameters that are related to this photochemical pollution episode during August 4-15, including 2-m air temperature, 2-m relative humidity, 10-m wind speed and 10-m wind direction at the meteorological sites of SH (31.40°N,121.46°E) located in Shanghai of SCR, HZ (30.23°N, 120.16°E) located in Hangzhou of CIR, and NJ (32.00°N, 118.80°E) located in Nanjing of NIR .

As shown in Fig. 3a, the hot weather at SH, HZ and NJ exists for nearly a week from August 7 to 12, with the hourly maximum temperature reaching the value over 40 ℃. Meanwhile, the variations of 2-m relative humidity show the negative correlation with those of 2-m air temperature. The minimum 2-m relative humidity at SH and HZ occur on August 9 and August 10 respectively, with the value below 75%. These minimum values are also lower than the values before and after the $O_3$ episode, suggesting that high-level $O_3$ episodes usually occur under the weather conditions with high temperature and low humidity. The value of 2-m relative humidity at NJ is relatively higher than those at SH and HZ and remains more stable. This extremely hot and dry weather condition at SH, HZ, and NJ are successively relieved on August 12, 13 and 15, which coincide well with the reduction of surface $O_3$ concentrations in Shanghai, Hangzhou, and Nanjing (Fig. 2). With respect to the observed surface wind (Fig. 3b), the 10-m wind speed at SH, HZ, and NJ is comparatively lower during the period of the $O_3$ episode, while it is suddenly intensified after August 12. Meanwhile, the wind direction is fluctuating from 7 to 12 August, while it maintains southeasterly wind after August 12 as well. The growth of wind speed is more distinct at

Atmos. Chem. Phys. Discuss., doi:10.5194/acp-2016-581, 2016
Manuscript under review for journal Atmos. Chem. Phys.
Published: 1 August 2016


Atmospheric Chemistry and Physics Discussions

SH, with the maximum value of approximately 9 m/s. The wind speed at NJ has an obviously diurnal variation from August 4 to 8, and the minimum value occurs on August 10.

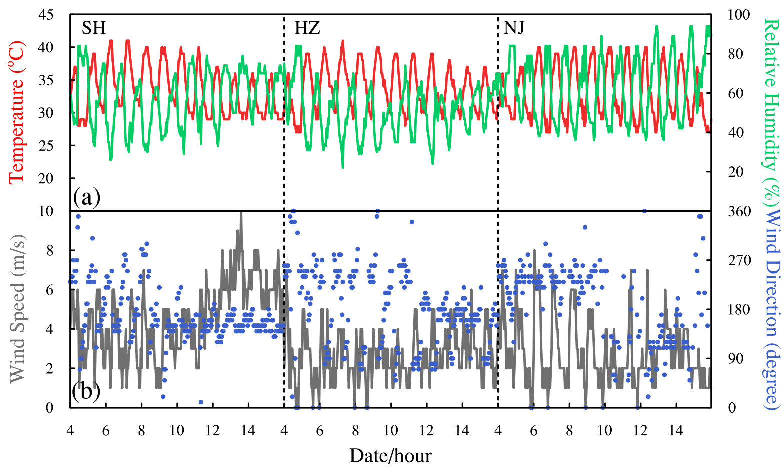


**Fig. 3. Temporal variations of the main meteorological parameters at SH (31.40°N,121.46°E), HZ (30.23°N, 120.16°E) and NJ (32.00°N, 118.80°E) meteorological stations during August 4-15, 2013: (a) 2-m air temperature (the red solid line) and 2-m relative humidity (the green solid line); (b) 10-m wind speed (the gray solid line) and 10-m wind direction (the blue scatter points).**

Fig. 4 displays the weather charts for the 500hPa layer over the East Asia at 00:00 (UTC) on 6, 8, 10, and 12 August 2013, which can illustrate the main synoptic patterns causing the $O_3$ pollution. Obviously, during the period of the selected $O_3$ episode, the whole YRD region is under the control of the strong Western Pacific subtropical high, which might be the direct and leading cause of the abnormal high temperature shown in Fig. 3a. The intensity of the subtropical high is usually characterized by the area index, defined as the total number of grid points that have geopotential heights of 588 decameters or greater in the region of 110-180°E and northward of 10°N. As shown in Fig. 4, the 588-decameter area covers most of southeast China, and the high pressure center (592-decameter area) is located in the southeastern coastal areas as well as the surrounding sea areas, which means the subtropical high is very intensive. This high pressure strengthens and remains over the YRD region for several days (from August 6 to 12), implying that the air subsides to the ground. The downward air acts as a dome capping the atmosphere, and helps to trap heat as well as air pollutants at the surface. Without the lift of air, there is little convection and therefore little cumulus clouds or rains. The end result is a continual accumulating of solar radiation and heat on the ground, which may greatly enhance the photochemical reactions between the abundant build-up air pollutants.

The other weather system worthy of note is Typhoon Utor (shown in Fig. 4c and d). Typhoon Utor is one of the strongest typhoons in the 2013 Pacific typhoon season, with the international code of 1311. It is formed early on August 8, develops into a tropical storm on August 9, undergoes a explosive intensification within a half of day, and achieves typhoon status on early August 10. After landing in Luzon of the Philippines on late August 11, it reemerges in the South China Sea on August 12. Typhoon Utor hits the land of Guangdong Province in China on August 14, and thereby is finally weakened into a tropical storm. In the end, it is ultimately dissipated on August 18. It was reported that ozone episodes during the hot season are usually associated with the passage of tropical cyclones close to the territory (Huang et al., 2005; Wang et al., 2006b; Jiang et al., 2008; Cheng et al., 2014; Hung and Lo, 2015). When a site is at the front of moving typhoon system, it can be controlled by the downward airflow induced by the typhoons' peripheral circulation. So, the typhoon system can cause the local weather around the site with high temperature, low humidity, strong solar radiation and small wind for a short time, before it is close enough to bring winds and rains. All these changes of meteorological conditions can significantly affect the formation of severe continuous $O_3$ pollution (Jiang et al., 2008). In this $O_3$ episode, the YRD region may be influenced by the peripheral circulation of Typhoon Utor as well. Especially on August 10-11, the downward airflow in the troposphere is significantly strengthened (shown in Fig. 6 and detailedly discussed in Sect. 4.2), which may enhance the build-up of heat and air pollutants and thereby result in worse air pollution shown in Fig. 2.

Moreover, from August 12 to 14 (shown in Fig. 4d), with the approaching of Typhoon Utor, the near-surface breeze over the YRD region gradually turns to be the prevailing southeasterly or southerly wind, with the highest wind speed up to 6-10 m/s in Shanghai. The strengthened wind can bring the clean marine air from ocean to inland, and thereby effectively mitigate the $O_3$ pollution. Meantime, Typhoon Utor also gradually affects the position and strength of the Western Pacific subtropical high. As the typhoon continuous approaching and finally landing on Guangdong, the high pressure system is forced to retreat easterly and move northwards. When the high pressure center completely moves to the oceans, the YRD region is totally under the control

Atmos. Chem. Phys. Discuss., doi:10.5194/acp-2016-581, 2016
Manuscript under review for journal Atmos. Chem. Phys.
Published: 1 August 2016


of the typhoon system. In the end, the hot weather is relieved and the $O_3$ pollution is mitigated. The coastal cities in CSR are closer to the typhoon system, so they are firstly influenced during this period. Thus, the wind at SH in CSR firstly changes, followed by HZ in CIR and NJ in NIR. In the same way, 2-m air temperature and $O_3$ concentrations also successively decrease from southeast (SH in CSR) to northwest (NJ in NIR) owing to the scavenging effect.

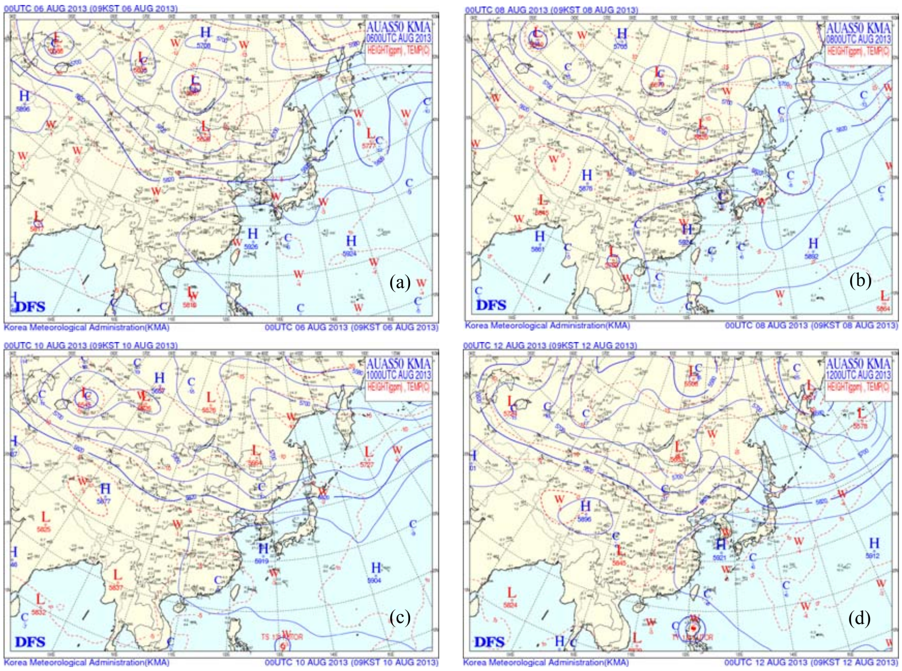


**Fig. 4. Weather charts at the 500hPa layer over the East Asia at 00:00 (UTC) on (a) August 6, (b) August 8, (c) August 10, and (d) August 12 2013 (from Korea Meteorological Administration)**

## 4 Modeling results and discussions

### 4.1 Evaluation of model performance

To evaluate the simulation performance, the hourly modeling results during the period of 4-15 August 2013 are compared with the observation records. Table 3 presents the performance statistics, including the values of the correlation coefficient (R), the normalized mean bias (NMB), and the root-mean-square error (RMSE), which are all calculated for 2-m air temperature ($T_2$), 2-m relative humidity ($RH_2$), surface ozone concentrations ($O_3$), and surface nitrogen dioxide concentrations ($NO_2$) in Shanghai (SH), Nanjing (NJ), and Hangzhou (HZ).

Atmos. Chem. Phys. Discuss., doi:10.5194/acp-2016-581, 2016
Manuscript under review for journal Atmos. Chem. Phys.
Published: 1 August 2016


Atmospheric Chemistry and Physics
Discussions

As indicated in Table 3, the simulated results of surface air temperature and relative humidity from WRF show good correlation with the observations. The highest correlation coefficient of 2-m air temperature ($T_2$) is found to be 0.91 at SH, followed by 0.84 at NJ and 0.80 at HZ (statistically significant at 95% confident level). The corresponding correlation coefficients for 2-m relative humidity ($RH_2$) are 0.85, 0.83 and 0.78, respectively. The values of RMSE for $T_2$ at SH, NJ and HZ are 4.15, 2.91and 3.09°C, and those for $RH_2$ are 19.3%, 9.41% and 13.96% respectively. However, our simulation underestimates $T_2$ and overestimates $RH_2$ to some certain extent, with the values of NMB for $T_2$ at SH, NJ and HZ being -11.69%, -5.98% and -6.53%, and those for $RH_2$ being 12.64%, 4.52% and 16.36%. These biases might be attributed to the uncertainty caused by the SLAB scheme, which can underestimate temperature in summer (Liao et al., 2014). According to the relevant studies (Li et al., 2012; Liao et al., 2015; Xie et al., 2016a), this level of over- or under-estimation is still acceptable. In summary, the abovementioned performance statistics numbers basically illustrate that the WRF simulation can reflect the major characteristics of meteorological conditions during this $O_3$ episode, and the meteorological outputs can be used in the pollutant concentration simulation.

**Table 3. Comparisons between the simulations and the observations at Shanghai, Nanjing and Hangzhou stations.**

| Sites [a] | Vars [b] | Mean | | R [e] | NMB [f] | RMSE [g] |
|---|---|---|---|---|---|---|
| | | OBS [c] | SIM [d] | | | |
| SH | $T_2$ (°C) | 33.27 | 31.38 | 0.91 | -11.69% | 4.15 |
| | $RH_2$ (%) | 57.91 | 65.23 | 0.85 | 12.64% | 19.3 |
| | $O_3$ (ppb) | 87.77 | 82.5 | 0.81 | -6.00% | 38.79 |
| | $NO_2$ (ppb) | 29.01 | 38.25 | 0.54 | 38.75% | 28.95 |
| NJ | $T_2$ (°C) | 32.95 | 30.98 | 0.84 | -5.98% | 2.91 |
| | $RH_2$ (%) | 63.28 | 66.14 | 0.83 | 4.52% | 9.41 |
| | $O_3$ (ppb) | 69.7 | 78.15 | 0.81 | 26.47% | 36.8 |
| | $NO_2$ (ppb) | 41.44 | 40.09 | 0.61 | -3.26% | 22.4 |
| HZ | $T_2$ (°C) | 33.25 | 31.08 | 0.8 | -6.53% | 3.09 |
| | $RH_2$ (%) | 52.76 | 61.39 | 0.78 | 16.36% | 13.96 |
| | $O_3$ (ppb) | 76.57 | 84.51 | 0.83 | 10.37% | 33.95 |
| | $NO_2$ (ppb) | 31.06 | 27.21 | 0.66 | -12.40% | 16.86 |

[a] Sites indicates the city where the observation sites locate, including Shanghai (SH), Nanjing (NJ), and Hangzhou (HZ); [b] Vars indicates the variables under validation, including 2-m air temperature ($T_2$), 2-m relative humidity ($RH_2$), ozone ($O_3$), and nitrogen dioxide ($NO_2$). The words between the parentheses behind variables indicate the

Atmos. Chem. Phys. Discuss., doi:10.5194/acp-2016-581, 2016
Manuscript under review for journal Atmos. Chem. Phys.
Published: 1 August 2016


Atmospheric Chemistry and Physics
Discussions

unit; [c] OBS indicates the observation data; [d] SIM indicates the simulation results from WRF/Chem; [e] R indicates the correlation coefficients, with statistically significant at 95% confident level; [f] NMB indicates the normalized mean bias; [g] RMSE indicates the root-mean-square error.

Fig. 5 shows the comparisons between the model results from CMAQ and the observed hourly concentrations of $O_3$ in Shanghai, Nanjing, Hangzhou and Wuxi during 4-15 August 2013. Obviously, the observations and the simulated results present reasonable agreement at each site, with the correlation coefficients of 0.81 to 0.83, NMB of -6% to 26.47%, RMSE of 33.95 to 38.79 ppb. Moreover, the simulation also reproduces the diurnal variation of $O_3$, which shows that the concentration reaches its maximum at around noon time and gradually decreases to its minimum after midnight. With respect to the $O_3$ precursor, comparisons of $NO_2$ concentrations between simulation results and observations show that the correlation coefficient at each city is about 0.6 (given in Table 3), which further prove that the process of $O_3$ formation is captured reasonable well over the YRD region and throughout the episode. However, CMAQ overestimates $NO_2$ and underestimates $O_3$ in Shanghai, while underestimates $NO_2$ and overestimates $O_3$ in Nanjing and Hangzhou. These biases of $O_3$ and $NO_2$ can be attributed to the uncertainties related with $O_3$ precursor emissions, meteorology, and observation deviation (Li et al., 2012). Moreover, the uncertainty in nonlinear chemical reactions coupled in CMAQ may also have important effects on model predictions. For example, the modeling results cannot catch the low $O_3$ values observed at night in Nanjing (Fig. 4b), Hangzhou (Fig. 4c) and Wuxi (Fig. 4d), implying there may be some imperfections in the nocturnal chemistry of CMAQ. Nevertheless, the performance of CMAQ model is comparable to the other applications (Goncalves et al., 2009; Li et al., 2012; Zhu et al., 2016). Compared to these previous related studies, the simulation in this study attains an acceptable and satisfactory result. Thus, the consistency of simulation and observation demonstrates that the modeling results are capable of capturing and reproducing the characteristics and changes of photochemical pollutants, and can be used to provide valuable insights into the governing processes of this $O_3$ episode.

Atmos. Chem. Phys. Discuss., doi:10.5194/acp-2016-581, 2016
Manuscript under review for journal Atmos. Chem. Phys.
Published: 1 August 2016


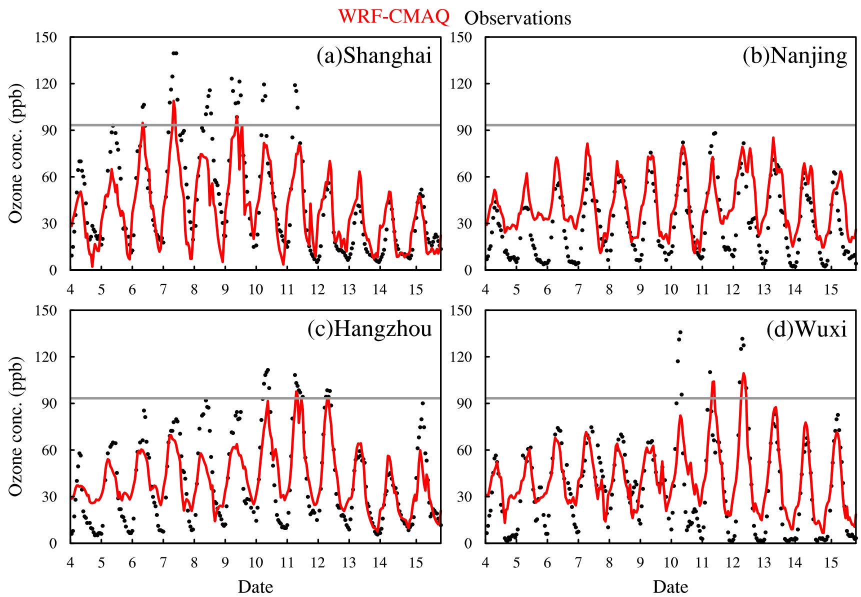


**Fig. 5. Hourly variations of the observed and the simulated $O_3$ concentrations in (a) Shanghai (SH), (b) Nanjing (NJ), (c) Hangzhou (HZ), and (d) Wuxi. In (a), (b), (c), and (d), the red solid lines show the modeling results, the black dot lines give the observations, and the solid gray lines represent the national standard for the hourly $O_3$ concentration, which is 200μg/m$^3$.**

### 4.2 Characteristics of the vertical airflows

Fig. 6 presents the vertical wind velocity as well as the vertical distribution of $O_3$ concentrations from 29.6°E to 34.7°E during August 7 - 12 2013. Along the vertical cross-section, the values from 118°E to 122°E are averaged in the meridional direction. The simulation results clearly illustrate that there are strong downward airflows over the YRD region during the period of the regional high-level $O_3$ pollution, which can be attributed to the fact that these areas are under the control of the subtropical high and the sinking airflow is predominant (as discussed in Sect. 3.2).

From 7 to 9 August 2013 (shown in Fig. 6a-c), except for the mentioned regional sinking airflows, there are still some local thermal circulations, which are related with urban heat islands, continually occurring at the lower atmospheric layers (< 2km) along the vertical cross-section of Hangzhou (HZ) - Shanghai (SH) - Nanjing (NJ). Usually high pressures are accompanied by more stagnant and fair dry weather, so the upward and the downward flows caused by urban-breeze

Atmos. Chem. Phys. Discuss., doi:10.5194/acp-2016-581, 2016
Manuscript under review for journal Atmos. Chem. Phys.
Published: 1 August 2016


circulations can easily appear in the urban areas of SH, HZ, and NJ. With respect to $O_3$, high concentrations (> 60ppb) usually appear from the surface to 1.5km height, with the maximum values over 70 ppb in and around cities. As discussed in Sect. 3.2, induced by the regional sinking airflows, air pollutants are tend to be trapped on the ground. Moreover, the local circulations over the cities (Fig. 6) make the urban areas to be the convergence zones, and thereby more air pollutants can be accumulated in and around these cities. Under the weather conditions induced by the subtropical high, such as high air temperature, stronger solar radiation and less water vapor, the chemical reactions between the build-up air pollutants can be enhanced to form the high-level $O_3$ pollution.

However, from 10 to 12 August, with the approaching of Typhoon Utor, the vertical air movements over the YRD region are not restricted at the lower atmosphere any more. As shown in Fig. 6d and e (August 10 and 11), there are stronger downward airflows from the surface to the top of troposphere. As discussed in Sect. 3.2, SH, HZ, and NJ are at the front of the moving typhoon system, so the peripheral circulation of Typhoon Utor may enhance the sinking of atmosphere, which can lead to higher air temperature, lower humidity, and stronger solar radiation. Affected by the enhanced downward air movement as well as the relevant changes of meteorological conditions, $O_3$ concentrations over the YRD region maintain a high pollution level, with the $O_3$ concentrations over 60 ppb below the height of 1.5 km. Furthermore, as shown in Fig. 6d to f, the high value center of $O_3$ concentrations moves from southeast to northwest during August 10 - 12, implying that the peripheral circulation of Typhoon Utor can drive the air from the coastal areas to the inland areas.

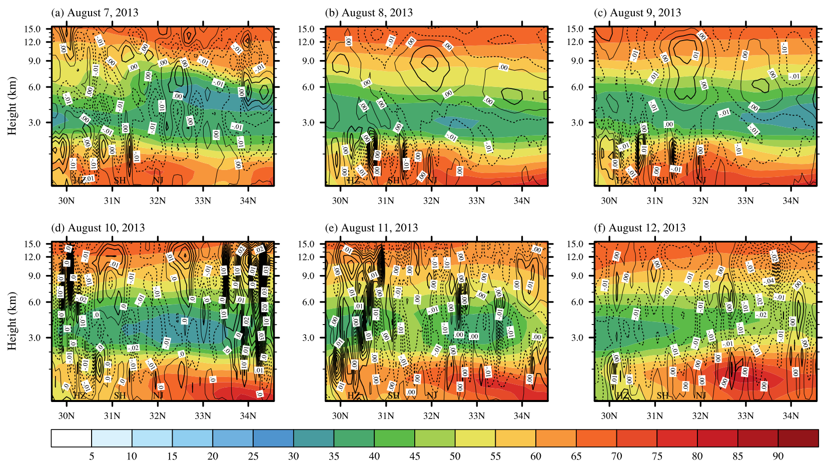


**Fig. 6. Simulated vertical wind velocity and vertical distribution of $O_3$ concentrations in the YRD region from 29.6°E to 34.7°E during 7 to 12 August 2013, with the values averaged in the meridional direction from 118°E to 122°E. The marks of HZ, SH, and NJ point out the latitudes of Hangzhou, Shanghai, and Nanjing, respectively.**

The vertical changes of wind velocity and $O_3$ concentrations above Shanghai are further illustrated in Fig. 7. Similar to that in Fig. 6, the atmospheric subsidence can also be found in the boundary layer of Shanghai during the period of the high-level $O_3$ pollution (from 7 to 12 August). Affected by the extremely high temperature, more active photochemical reactions lead to higher $O_3$ concentrations in the whole atmospheric boundary layer. The downward airflows induced by the subtropical high trap and enhance the accumulation of surface $O_3$ as time passes. Thus, high $O_3$ concentrations are formed below 2 km above the urban areas of Shanghai, and the high concentration centers occur near the surface below 500 m. It is interesting that $O_3$ concentration on August 8 is comparatively lower, which can be seen in Fig. 2 as well. This phenomenon can be explained by the fact shown in Fig. 7 that the transient upward airflow occurs at above 300 m over Shanghai and inhibits the accumulation of the $O_3$ pollution at the surface. Additionally, Fig. 7 also presents the possible effects of Typhoon Utor on the formation of $O_3$. On August 10, when the typhoon system approaches to the eastern coastal areas of China, the sinking air above Shanghai is apparently strengthened, and thereby enhances the intensity of $O_3$ pollution as well as the scope of the pollution. But after August 12, when Typhoon Utor changes the wind and even impacts the subtropical high, high temperature is alleviated and the build-up $O_3$ is transported to other places.

Atmos. Chem. Phys. Discuss., doi:10.5194/acp-2016-581, 2016
Manuscript under review for journal Atmos. Chem. Phys.
Published: 1 August 2016


Thus, the pollution is mitigated.

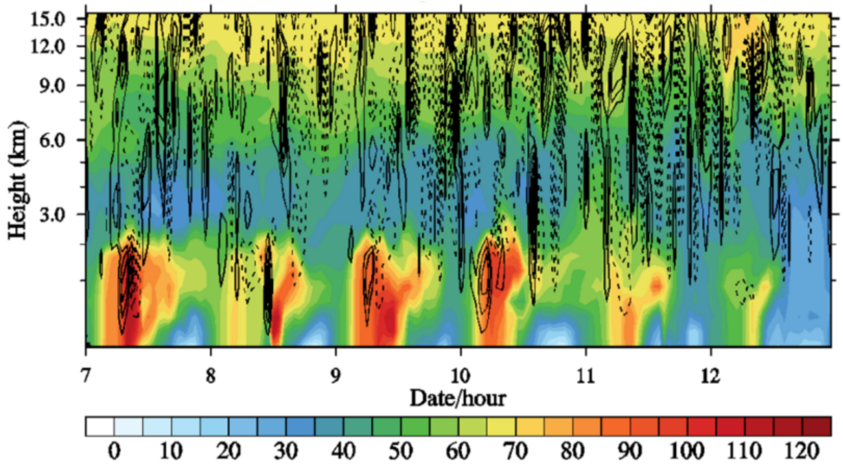


**Fig. 7. Temporal variations for the vertical wind velocity and the vertical distribution of $O_3$ concentrations above Shanghai (SH) during August 7 to 12, 2013.**

### 4.3 Process analysis for ozone formation

#### 4.3.1 Typical cities in the YRD region

Fig. 8 shows the daily contributions of different atmospheric processes to the formation of $O_3$ in Shanghai (SH), Nanjing (NJ), and Hangzhou (HZ) at the first modeling layer from 4 to 15 August 2013. As shown in the figure, for all cities during this period, the major contributors to high $O_3$ concentrations include the vertical diffusion (VDIF), the dry deposition (DDEP), the gas-phase chemistry (CHEM), and the total advection (TADV). TADV is the sum of the horizontal advection (HADV) and the vertical advection (ZADV). In this study, HADV and ZADV are considered together as TADV because they are inevitably linked as the inseparable parts of air circulation. As discussed in Sect. 3.2, the strong sinking air causes slow wind on the ground and little clouds in the sky, so the contributions of horizontal diffusion (HDIF) and cloud processes (CLDS) are quite small during this episode.

In the first layer of the urban areas of Shanghai (Fig. 8a), the averaged daily contributions during 4-15 August for the vertical diffusion (VDIF), the gas-phase chemistry (CHEM), the advection processes (TADV) and the dry deposition (DDEP) are 9.95, 10.10, -11.74 and -7.28 ppb/h, respectively. Obviously, VDIF and CHEM exhibit significant positive contributions to $O_3$

during most days, while TADV and DDEP mainly show the consumption contributions. The sinking air caused by the weather system discussed in Sect. 3.2 can trap heat and air pollutants on the ground, and results in VDIF to be the most import source of surface $O_3$. Meanwhile, the hotter and dryer weather with more sunshine, which is related with the sinking air, can enhance the photochemical reactions. So, CHEM can form more $O_3$ on the ground. Compared with the time series of CHEM and DDEP in which there are no obvious fluctuations, the values of VDIF and TADV significantly change with the time, with the daily mean contributions varying from 3.99 to 28.45 ppb/h for VDIF and from -2.56 to -28.13 ppb/h for TADV. These time variations should be related with the changes of vertical air movement. For example, the value of VDIF on August 8 is only 3.99 ppb/h, which can be attributed to the local transient upward airflow over Shanghai (shown in Fig. 7). On August 10, however, VDIF can contribute 28.45 ppb $O_3$ per hour, which may be related with the enhanced downward air movement caused by the peripheral circulation of Typhoon Utor. Moreover, during the high-level $O_3$ episode from August 7-12, the mean values for VDIF, CHEM, TADV and DDEP are 13.41, 11.21, -8.37 and -14.74 ppb/h. But after August 12, the mean contributions of VDIF, CHEM, TADV and DDEP decrease to 5.35, 9.53, -5.52 and -10.85 ppb/h. These reductions should be related with the process that the subtropical high moves eastward and northward forced by Typhoon Utor. By quantifying the relative importance of each process to $O_3$ formation, the IPR analysis provides a fundamental explanation for the synthetically influence of the high pressure and the typhoon system, which has been discussed in Sect. 3.2 and 4.1, and further illustrates the exact mechanism.

Fig. 8b presents the result of IPR analysis for Hangzhou. During 4-15 August, VDIF and CHEM are the major source of surface $O_3$ with the average contribution of 5.36 ppb/h for VDIF and 10.97 ppb/h for CHEM, while TADV and DDEP are two important sinks for $O_3$ with the average contribution of -9.63 ppb/h for TADV and -5.14 ppb/h for DDEP. Synthetically impacted by Western Pacific subtropical high and Typhoon Utor, the mean contributions during the $O_3$ episode (from August 7 to August 12) for VDIF, CHEM, TADV and DDEP increase to 7.21, 12.61, -11.51 and -5.92 ppb/h, respectively. The highest VDIF contribution occurs on August 10-11, which may be attributed to the effect of typhoon's peripheral circulation, implying Typhoon Utor also plays an essential role in the formation of $O_3$ pollution in Hangzhou. After Typhoon Utor approach close enough to Hangzhou, the mean values of VDIF, CHEM, TADV and DDEP finally decrease to 4.84, 10.08, -8.92 and -4.78 ppb/h, respectively. In a word, Hangzhou is located close to Shanghai, so the temporal variations of VDIF, CHEM, TADV and DDEP in Hangzhou are similar to those in Shanghai.

However, the similar variation pattern of VDIF, CHEM, TADV and DDEP occurring in Shanghai and Hangzhou does not appear in Nanjing. As shown in Fig. 8c, the mean contributions of VDIF, CHEM, TADV and DDEP to surface $O_3$ in Nanjing are 11.31, 9.55 -1.34 and -17.57 ppb/h during the whole period, while the values during 7- 12 August are 10.32, 10.70, -0.99 and -18.42 ppb/h. There are no apparent fluctuations or sudden increases of these contributors during the period from August 4 to 15, implying Nanjing is generally under the control of the Western Pacific subtropical high and can hardly be affected by the typhoon system. As a typical city in the northwest inland area of the YRD region (NIR), Nanjing is located far away from the sea, which means it may not be easily affected by the weather system from the ocean.

Additionally, at the altitude of 500 m and 1500 m above Shanghai, Nanjing, and Hangzhou (not shown), CHEM is also the major contributor to $O_3$ formation, with the values a litter lower than those at the surface, suggesting that there are strong photochemical reactions in the whole boundary layer of these YRD cities. In contrast, VDIF has an opposite effect in the middle of the boundary layer, with the negative contributions for $O_3$ of -3.26 ppb/h in Shanghai, -2.37 ppb/h in Hangzhou, and -3.21 ppb/h in Nanjing, respectively (not shown). The loss of $O_3$ at higher atmospheric level caused by VDIF further proves the essential role of the downward vertical movement in this $O_3$ episode.

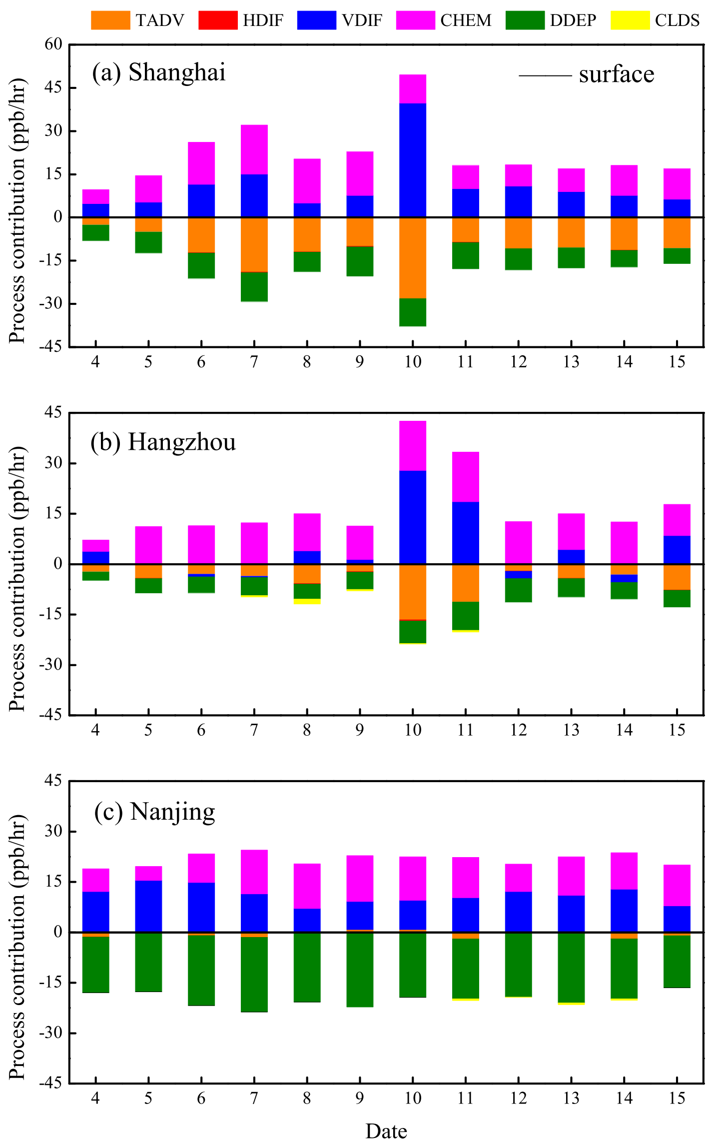


**Fig. 8. Variations of the daily mean values for the contributions of individual processes to $O_3$ formation in (a) Shanghai, (b) Hangzhou, and (c) Nanjing from 4 to 15 August 2013 at the surface layer. The contributors include the total advection (TADV), the horizontal diffusion (HDIF), the vertical diffusion (VDIF), the gas-phase chemistry (CHEM), the dry deposition (DDEP), and the cloud processes with the aqueous chemistry (CLDS).**

### 4.3.2 Spatial distribution of the contributors for the $O_3$ episode over the YRD region

Fig. 9 demonstrates the spatial distribution of the mean contributions of main processes

Atmos. Chem. Phys. Discuss., doi:10.5194/acp-2016-581, 2016
Manuscript under review for journal Atmos. Chem. Phys.
Published: 1 August 2016


Atmospheric Chemistry and Physics
Discussions

(TADV, VDIF, DDEP and CHEM) to the formation of this high-level $O_3$ episode at the lowest modeling layer in domain 3. The modeling results from 7 to 12 August are averaged to provide the mean values.

Similar to the results shown in Fig. 8, Fig. 9 illustrates that the vertical diffusion (VDIF) and the gas-phase chemistry (CHEM) exhibit significant positive contributions to $O_3$ over the YRD region and the surrounding areas during the high-level $O_3$ episode. The contributions of VDIF in domain 3 (Fig. 9a) range from 5 to 25 ppb/h, with the high values (> 20 ppb/h) occurring in the southeast coastal areas. For CHEM (Fig. 9b), the contributions vary within the range of 0-15 ppb/h, with the high values over 10 ppb/h appearing in and around the big cities. As discussed above, these regional positive contributions of VDIF and CHEM over domain 3 should be related to the facts that the whole region is under the control of the Western Pacific subtropical high. With respect to the higher contributions of CHEM in the urban areas, they should be attributed to the spatial distribution of the emissions of $O_3$ precursors, which is also higher in the cities. Furthermore, higher air temperature in the cities related with the urban heat island may enhance the chemical reactions and form more $O_3$ in these areas as well.

As shown in Fig. 9c, DDEP is the main critical factor of the consumption of $O_3$, with the negative contributions varying from 0 to -25 ppb/h over the modeling domain 3. Small values usually occur on the water, which may be related with less air pollution over rivers, lakes and oceans. High values can be found on land, especially in the southeast coastal areas. For the contributions of TADV (Fig. 9d), the values in domain 3 range from -10 to 10 ppb/hr, with the positive contributions generally occurring on land while the negative (consuming) ones appearing on the water. The maximum positive contributions of TADV are usually found along the boundary between the land and the water, which should be explained by the facts that the land-sea breeze circulations can play an important role in the redistribution of the formed $O_3$.

In all, more active photochemical reactions and the vertical diffusion play a significant role in the accumulation of surface $O_3$, and lead to the high-level $O_3$ pollution episode over the YRD region. The major driving factor should be the Western Pacific subtropical high. Moreover, the contributions of VDIF, DDEP and CHEM exhibit a similar spatial pattern with the high values mostly concentrate in the southeast coastal areas, implying the Typhoon Utor also plays a collaborative effect. The details and the processes of the synthetical effects of high pressure and

Atmos. Chem. Phys. Discuss., doi:10.5194/acp-2016-581, 2016
Manuscript under review for journal Atmos. Chem. Phys.
Published: 1 August 2016

Atmospheric Chemistry and Physics Discussions

typhoon system have been discussed in Sect. 3.2, 4.2 and 4.3.1.

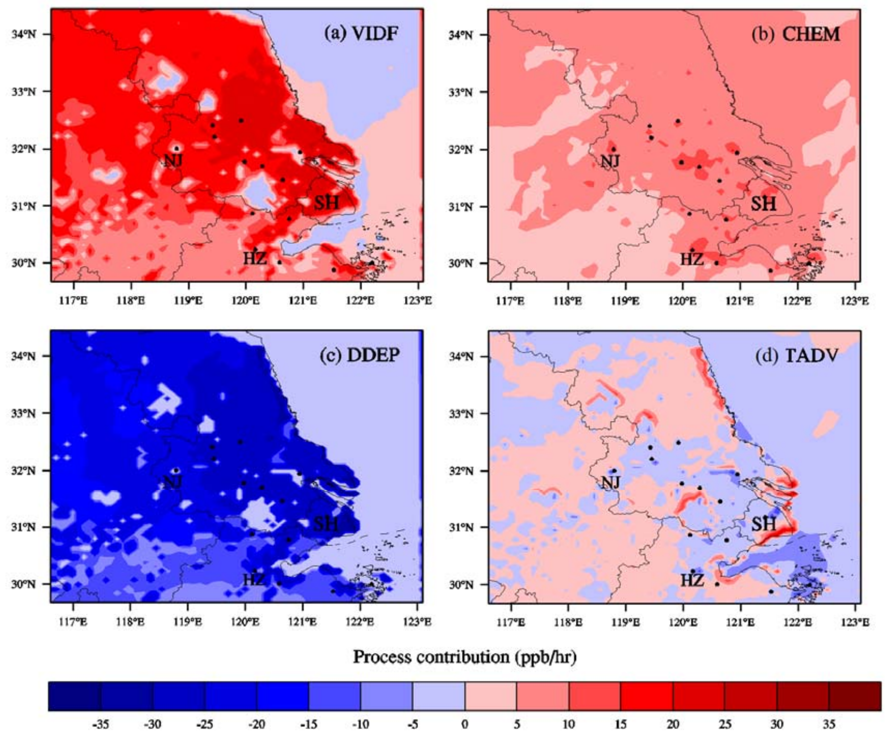


**Fig. 9. The contributions of main processes to $O_3$ formation over the YRD region, including (a) gas chemistry (CHEM), (b) vertical diffusion (VDIF), (c) dry deposition (DDEP), and (d) total advection (TADV). The values are averaged from 7 to 12 August 2013.**

## 5. Conclusions

By means of observational analysis and numerical simulation, the characteristics and the essential impact factors of a typical regional continuous $O_3$ pollution over the YRD region is investigated. Base on the observation data, it is found that this high-level $O_3$ episode lasts for nearly a week from 7 to 12 August 2013, with the $O_3$ concentration exceeding the national air quality standard in more than half of the cities over the YRD region. In the cities of Jiaxing, Changzhou and Nantong, high $O_3$ concentrations can reach the values over 160 ppb. Fine weather conditions, such as extremely high temperature, low relative humidity, and weak wind speed, provide a favorable atmospheric environment for the complicated photochemical reactions and help to form $O_3$. The analysis of weather systems and the modeling results from WRF/CMAQ all illustrate that the continuous strong Western Pacific subtropical high is the leading factor of the abnormal high temperature weather and the heavy $O_3$ pollution, by inducing more sinking air to trap heat as well as air pollutants at the surface. The development of this episode is closely related to the movement of Typhoon Utor as well. The temporal variations of the vertical wind velocity and $O_3$ concentrations show that when the YRD region is at the front of moving typhoon system, the downward airflow is enhanced in the boundary layer with fine weather, and thereby the air pollutants are trapped and accumulated near the surface. Moreover, in the last stage of the $O_3$ episode, the activity of Typhoon Utor weakens the strength of the subtropical high and forces it to retreat easterly and move northward, and the prevailing southeasterly surface wind related with the approaching of Typhoon Utor contributes to the mitigation of the $O_3$ pollution.

The Integrated Process Rate (IPR) analysis implemented in CMAQ is specially carried out to quantify the relative contributions of individual processes and give a fundamental explanation. Over the YRD region, during the high-level $O_3$ episode from August 7-12, the vertical diffusion (VDIF) and the gas-phase chemistry (CHEM) exhibit significant positive contributions to surface $O_3$, with the high values over 20 ppb/h for VDIF and over 10 ppb/h for CHEM. The total advection (TADV) can give the positive contribution on land and the negative contribution on the water. The dry deposition (DDEP) is the major sink of surface $O_3$, while the contributions of horizontal diffusion (HDIF) and cloud processes (CLDS) are quite small. To some extent, the distribution pattern reflects the heterogeneity of emissions and the effects of weather system. Influenced by the sinking air as well as the fine weather induced by the Western Pacific subtropical high, the contributions of VDIF and CHEM to surface $O_3$ maintain the high values of 13.41 and 11.21 ppb/h for Shanghai, 7.21 and 12.61 ppb/h for Hangzhou, and 10.32 and 10.70 ppb/h for Nanjing, respectively. Moreover, on August 10-11, the cities close to the sea are apparently affected by the periphery circulation of Typhoon Utor, with the contribution of VDIF increase to 28.45 ppb/h in Shanghai and 19.76 ppb/h in Hangzhou. When the typhoon system significantly weaken the high pressure system, the contributions of VDIF, CHEM, TADV and DDEP decrease to a low level in all cities.

WRF-CMAQ model system shows a relatively good performance in simulation of the $O_3$ episode, with the simulated meteorological conditions and air pollutant concentrations basically in agreement with the observations in most YRD cities. Our results in this study can provide an insight for the formation mechanism of regional $O_3$ pollution in East Asia, and help to forecast the $O_3$ pollution synthetically impacted by the Western Pacific subtropical high and the tropical cyclone system.

**Acknowledgments**

This study was supported by the National Natural Science Foundation of China (41475122, 91544230, 41575145), the National Special Fund for Environmental Protection Research in the Public Interest (201409008), EU 7th Framework Marie Curie Actions IRSES project REQUA (PIRSES-GA-2013-612671), and the National Science Foundation of Jiangsu Provence (BE2015151). The authors would like to thank Xiaoxun Xie for preliminary data processing, and the anonymous reviewers for their constructive and precious comments on this manuscript.

**References**

An, X., Zhu, T., Wang, Z., Li, C., and Wang, Y.: A modeling analysis of a heavy air pollution episode occurred in Beijing, Atmos Chem Phys, 7, 3103-3114, 2007.

Byun, D., and Schere, K. L.: Review of the governing equations, computational algorithms, and other components of the models-3 Community Multiscale Air Quality (CMAQ) modeling system, Appl Mech Rev, 59, 51-77, 10.1115/1.2128636, 2006.

Chan, C. K., and Yao, X.: Air pollution in mega cities in China, Atmos Environ, 42, 1-42, 10.1016/j.atmosenv.2007.09.003, 2008.

Chen, F., and Dudhia, J.: Coupling an advanced land surface-hydrology model with the Penn State-NCAR MM5 modeling system. Part I: Model implementation and sensitivity, Mon Weather Rev, 129, 569-585, Doi 10.1175/1520-0493(2001)129<0569:Caalsh>2.0.Co;2, 2001.

Chen, D., Zhou, B., Beirle, S., Chen, L. M., and Wagner, T.: Tropospheric NO2 column densities deduced from zenith-sky DOAS measurements in Shanghai, China, and their application to satellite validation, Atmos Chem Phys, 9, 3641-3662, 2009.

Cheng, W. L., Lai, L. W., Den, W., Wu, M. T., Hsueh, C. A., Lin, P. L., Pai, C. L., and Yan, Y. L.: The relationship between typhoons' peripheral circulation and ground-level ozone concentrations in central Taiwan, Environ Monit Assess, 186, 791-804, 10.1007/s10661-013-3417-7, 2014.

Chiqueto, J., Silva, M. E. S.: São Paulo "Surface Ozone Layer" and the atmosphere: characteristics of tropospheric ozone concentrations in the city and how the atmosphere influences them, VDM Verlag Dr. Muller, Saarbrücken, 2010.

Ding, A. J., Fu, C. B., Yang, X. Q., Sun, J. N., Zheng, L. F., Xie, Y. N., Herrmann, E., Nie, W., Petaja, T., Kerminen, V. M., and Kulmala, M.: Ozone and fine particle in the western Yangtze River Delta: an overview of 1 yr data at the SORPES station, Atmos Chem Phys, 13, 5813-5830, 10.5194/acp-13-5813-2013, 2013.

Duan, J. C., Tan, J. H., Yang, L., Wu, S., and Hao, J. M.: Concentration, sources and ozone formation potential of

Atmos. Chem. Phys. Discuss., doi:10.5194/acp-2016-581, 2016
Manuscript under review for journal Atmos. Chem. Phys.
Published: 1 August 2016


Atmospheric Chemistry and Physics
Open Access
Discussions

volatile organic compounds (VOCs) during ozone episode in Beijing, Atmos Res, 88, 25-35, 10.1016/j.atmosres.2007.09.004, 2008.

Emmons, L. K., Walters, S., Hess, P. G., Lamarque, J. F., Pfister, G. G., Fillmore, D., Granier, C., Guenther, A., Kinnison, D., Laepple, T., Orlando, J., Tie, X., Tyndall, G., Wiedinmyer, C., Baughcum, S. L., and Kloster, S.: Description and evaluation of the Model for Ozone and Related chemical Tracers, version 4 (MOZART-4), Geosci Model Dev, 3, 43-67, 2010.

Fann, N., and Risley, D.: The public health context for PM2.5 and ozone air quality trends, Air Qual Atmos Hlth, 6, 1-11, 10.1007/s11869-010-0125-0, 2013.

Feng, Z. W., Jin, M. H., Zhang, F. Z., and Huang, Y. Z.: Effects of ground-level ozone (O-3) pollution on the yields of rice and winter wheat in the Yangtze River Delta, J Environ Sci-China, 15, 360-362, 2003.

Foley, K. M., Roselle, S. J., Appel, K. W., Bhave, P. V., Pleim, J. E., Otte, T. L., Mathur, R., Sarwar, G., Young, J. O., Gilliam, R. C., Nolte, C. G., Kelly, J. T., Gilliland, A. B., and Bash, J. O.: Incremental testing of the Community Multiscale Air Quality (CMAQ) modeling system version 4.7, Geosci Model Dev, 3, 205-226, 2010.

Gao, J. H., Bin, Z., Xiao, H., Kang, H. Q., Hou, X. W., and Shao, P.: A case study of surface ozone source apportionment during a high concentration episode, under frequent shifting wind conditions over the Yangtze River Delta, China, Sci Total Environ, 544, 853-863, 10.1016/j.scitotenv.2015.12.039, 2016.

Geng, F. H., Tie, X. X., Xu, J. M., Zhou, G. Q., Peng, L., Gao, W., Tang, X., and Zhao, C. S.: Characterizations of ozone, NOx, and VOCs measured in Shanghai, China, Atmos Environ, 42, 6873-6883, 10.1016/j.atmosenv.2008.05.045, 2008.

Goncalves, M., Jimenez-Guerrero, P., and Baldasano, J. M.: Contribution of atmospheric processes affecting the dynamics of air pollution in South-Western Europe during a typical summertime photochemical episode, Atmos Chem Phys, 9, 849-864, 2009.

Grell, G. A., and Devenyi, D.: A generalized approach to parameterizing convection combining ensemble and data assimilation techniques, Geophys Res Lett, 29, Artn 169310.1029/2002gl015311, 2002.

Guo, H., Jiang, F., Cheng, H. R., Simpson, I. J., Wang, X. M., Ding, A. J., Wang, T. J., Saunders, S. M., Wang, T., Lam, S. H. M., Blake, D. R., Zhang, Y. L., and Xie, M.: Concurrent observations of air pollutants at two sites in the Pearl River Delta and the implication of regional transport, Atmos Chem Phys, 9, 7343-7360, 2009.

Han, S. Q., Bian, H., Feng, Y. C., Liu, A. X., Li, X. J., Zeng, F., and Zhang, X. L.: Analysis of the Relationship between O-3, NO and NO2 in Tianjin, China, Aerosol Air Qual Res, 11, 128-139, 10.4209/aaqr.2010.07.0055, 2011.

Hong, S. Y., Dudhia, J., and Chen, S. H.: A revised approach to ice microphysical processes for the bulk parameterization of clouds and precipitation, Mon Weather Rev, 132, 103-120, Doi 10.1175/1520-0493(2004)132<0103:Aratim>2.0.Co;2, 2004.

Hong, S. Y., Noh, Y., and Dudhia, J.: A new vertical diffusion package with an explicit treatment of entrainment processes, Mon Weather Rev, 134, 2318-2341, Doi 10.1175/Mwr3199.1, 2006.

Huang, J. P., Fung, J. C. H., Lau, A. K. H., and Qin, Y.: Numerical simulation and process analysis of typhoon-related ozone episodes in Hong Kong, J Geophys Res-Atmos, 110, Artn D0530110.1029/2004jd004914, 2005.

Huang, J. P., Fung, J. C. H., and Lau, A. K. H.: Integrated processes analysis and systematic meteorological classification of ozone episodes in Hong Kong, J Geophys Res-Atmos, 111, Artn D2030910.1029/2005jd007012, 2006.

Hung, C. H., and Lo, K. C.: Relationships between Ambient Ozone Concentration Changes in Southwestern Taiwan and Invasion Tracks of Tropical Typhoons, Adv Meteorol, Artn 40297610.1155/2015/402976, 2015.

Jenkin, M. E., and Clemitshaw, K. C.: Ozone and other secondary photochemical pollutants: chemical processes governing their formation in the planetary boundary layer, Atmos Environ, 34, 2499-2527, Doi 10.1016/S1352-2310(99)00478-1, 2000.

Jiang, F., Wang, T. J., Wang, T. T., Xie, M., and Zhao, H.: Numerical modeling of a continuous photochemical pollution episode in Hong Kong using WRF-chem, Atmos Environ, 42, 8717-8727, 10.1016/j.atmosenv.2008.08.034, 2008.

Jiang, F., Zhou, P., Liu, Q., Wang, T. J., Zhuang, B. L., and Wang, X. Y.: Modeling tropospheric ozone formation over East China in springtime, J Atmos Chem, 69, 303-319, 10.1007/s10874-012-9244-3, 2012.

Kim, H. J., and Wang, B.: Sensitivity of the WRF Model Simulation of the East Asian Summer Monsoon in 1993 to Shortwave Radiation Schemes and Ozone Absorption, Asia-Pac J Atmos Sci, 47, 167-180, 10.1007/s13143-011-0006-y, 2011.

Lam, K. S., Wang, T. J., Wu, C. L., and Li, Y. S.: Study on an ozone episode in hot season in Hong Kong and transboundary air pollution over Pearl River Delta region of China, Atmos Environ, 39, 1967-1977, 10.1016/j.atmosenv.2004.11.023, 2005.

Landry, J. S., Neilson, E. T., Kurz, W. A., and Percy, K. E.: The impact of tropospheric ozone on landscape-level merchantable biomass and ecosystem carbon in Canadian forests, Eur J Forest Res, 132, 71-81, 10.1007/s10342-012-0656-z, 2013.

Li, L., Chen, C. H., Huang, C., Huang, H. Y., Zhang, G. F., Wang, Y. J., Chen, M. H., Wang, H. L., Chen, Y. R., Streets, D. G., and Fu, J. M.: Ozone sensitivity analysis with the MM5-CMAQ modeling system for Shanghai, J Environ Sci-China, 23, 1150-1157, 10.1016/S1001-0742(10)60527-X, 2011.

Li, L., Chen, C. H., Huang, C., Huang, H. Y., Zhang, G. F., Wang, Y. J., Wang, H. L., Lou, S. R., Qiao, L. P., Zhou, M., Chen, M. H., Chen, Y. R., Streets, D. G., Fu, J. S., and Jang, C. J.: Process analysis of regional ozone formation over the Yangtze River Delta, China using the Community Multi-scale Air Quality modeling system, Atmos Chem Phys, 12, 10971-10987, 10.5194/acp-12-10971-2012, 2012.

Li, M. M., Song, Y., Huang, X., Li, J. F., Mao, Y., Zhu, T., Cai, X. H., and Liu, B.: Improving mesoscale modeling using satellite-derived land surface parameters in the Pearl River Delta region, China, J Geophys Res-Atmos, 119, 6325-6346, 10.1002/2014JD021871, 2014.

Li, M. M., Song, Y., Mao, Z. C., Liu, M. X., and Huang, X.: Impacts of thermal circulations induced by urbanization on ozone formation in the Pearl River Delta region, China, Atmos Environ, 127, 382-392, 10.1016/j.atmosenv.2015.10.075, 2016.

Liao, J. B., Wang, T. J., Wang, X. M., Xie, M., Jiang, Z. Q., Huang, X. X., and Zhu, J. L.: Impacts of different urban canopy schemes in WRF/Chem on regional climate and air quality in Yangtze River Delta, China, Atmos Res, 145, 226-243, 10.1016/j.atmosres.2014.04.005, 2014.

Liao, J. B., Wang, T. J., Jiang, Z. Q., Zhuang, B. L., Xie, M., Yin, C. Q., Wang, X. M., Zhu, J. L., Fu, Y., and Zhang, Y.: WRF/Chem modeling of the impacts of urban expansion on regional climate and air pollutants in Yangtze River Delta, China, Atmos Environ, 106, 204-214, 10.1016/j.atmosenv.2015.01.059, 2015.

Liu, X. H., Zhang, Y., Xing, J., Zhang, Q. A., Wang, K., Streets, D. G., Jang, C., Wang, W. X., and Hao, J. M.: Understanding of regional air pollution over China using CMAQ, part II. Process analysis and sensitivity of ozone and particulate matter to precursor emissions, Atmos Environ, 44, 3719-3727, 10.1016/j.atmosenv.2010.03.036, 2010.

Liu, Q., Lam, K. S., Jiang, F., Wang, T. J., Xie, M., Zhuang, B. L., and Jiang, X. Y.: A numerical study of the impact of climate and emission changes on surface ozone over South China in autumn time in 2000-2050, Atmos Environ, 76, 227-237, 10.1016/j.atmosenv.2013.01.030, 2013.

Lou, S. J., Liao, H., and Zhu, B.: Impacts of aerosols on surface-layer ozone concentrations in China through heterogeneous reactions and changes in photolysis rates, Atmos Environ, 85, 123-138, 10.1016/j.atmosenv.2013.12.004, 2014.

Lu, W. Z., and Wang, X. K.: Evolving trend and self-similarity of ozone pollution in central Hong Kong ambient during 1984-2002, Sci Total Environ, 357, 160-168, 10.1016/j.scitotenv.2005.03.015, 2006.

Ma, J. Z., Xu, X. B., Zhao, C. S., and Yan, P.: A review of atmospheric chemistry research in China: Photochemical smog, haze pollution, and gas-aerosol interactions, Adv Atmos Sci, 29, 1006-1026, 10.1007/s00376-012-1188-7, 2012.

Mlawer, E. J., Taubman, S. J., Brown, P. D., Iacono, M. J., and Clough, S. A.: Radiative transfer for inhomogeneous atmospheres: RRTM, a validated correlated-k model for the longwave, J Geophys Res-Atmos, 102, 16663-16682, Doi 10.1029/97jd00237, 1997.

Monin, A. S., Obukhov, A.M.: Basic laws of turbulent mixing in the surface layer of the atmosphere, Contributions of the Geophysical Institute of the Slovak Academy of Sciences 151, 163-187, 1954.

Ran, L., Zhao, C. S., Geng, F. H., Tie, X. X., Tang, X., Peng, L., Zhou, G. Q., Yu, Q., Xu, J. M., and Guenther, A.: Ozone photochemical production in urban Shanghai, China: Analysis based on ground level observations, J Geophys Res-Atmos, 114, Artn D1530110.1029/2008jd010752, 2009.

Shao, M., Zhang, Y. H., Zeng, L. M., Tang, X. Y., Zhang, J., Zhong, L. J., and Wang, B. G.: Ground-level ozone in the Pearl River Delta and the roles of VOC and NOx in its production, J Environ Manage, 90, 512-518, 10.1016/j.jenvman.2007.12.008, 2009.

Shi, C. Z., Wang, S. S., Liu, R., Zhou, R., Li, D. H., Wang, W. X., Li, Z. Q., Cheng, T. T., and Zhou, B.: A study of aerosol optical properties during ozone pollution episodes in 2013 over Shanghai, China, Atmos Res, 153, 235-249, 10.1016/j.atmosres.2014.09.002, 2015.

Sillman, S.: The relation between ozone, NOx and hydrocarbons in urban and polluted rural environments, Atmos Environ, 33, 1821-1845, Doi 10.1016/S1352-2310(98)00345-8, 1999.

State Environmental Protection Administration of China: China National Environmental Protection Standard: Automated Methods for Ambient Air Quality Monitoring, China Environmental Science Press, Beijing, 2006.

Tang, W. Y., Zhao, C. S., Geng, F. H., Peng, L., Zhou, G. Q., Gao, W., Xu, J. M., and Tie, X. X.: Study of ozone "weekend effect" in Shanghai, Sci China Ser D, 51, 1354-1360, 10.1007/s11430-008-0088-2, 2008.

Tang, G., Li, X., Wang, Y., Xin, J., and Ren, X.: Surface ozone trend details and interpretations in Beijing, 2001-2006, Atmos Chem Phys, 9, 8813-8823, 2009.

Tu, J., Xia, Z. G., Wang, H. S., and Li, W. Q.: Temporal variations in surface ozone and its precursors and meteorological effects at an urban site in China, Atmos Res, 85, 310-337, 10.1016/j.atmosres.2007.02.003, 2007.

Wang, H. X., Zhou, L. J., and Tang, X. Y.: Ozone concentrations in rural regions of the Yangtze Delta in China, J Atmos Chem, 54, 255-265, 10.1007/s10874-006-9024-z, 2006a.

Wang, T. J., Lam, K. S., Xie, M., Wang, X. M., Carmichael, G., and Li, Y. S.: Integrated studies of a photochemical smog episode in Hong Kong and regional transport in the Pearl River Delta of China, Tellus B, 58, 31-40, 10.1111/j.1600-0889.2005.00172.x, 2006b.

Wang, X. M., Lin, W. S., Yang, L. M., Deng, R. R., and Lin, H.: A numerical study of influences of urban land-use change on ozone distribution over the Pearl River Delta region, China, Tellus B, 59, 633-641, 10.1111/j.1600-0889.2007.00271.x, 2007.

Wang, T., Wei, X. L., Ding, A. J., Poon, C. N., Lam, K. S., Li, Y. S., Chan, L. Y., and Anson, M.: Increasing surface ozone concentrations in the background atmosphere of Southern China, 1994-2007, Atmos Chem Phys, 9, 6217-6227, 2009a.

Wang, X. M., Chen, F., Wu, Z. Y., Zhang, M. G., Tewari, M., Guenther, A., and Wiedinmyer, C.: Impacts of

Atmos. Chem. Phys. Discuss., doi:10.5194/acp-2016-581, 2016
Manuscript under review for journal Atmos. Chem. Phys.
Published: 1 August 2016


Atmospheric Chemistry and Physics Discussions
Open Access

Weather Conditions Modified by Urban Expansion on Surface Ozone: Comparison between the Pearl River Delta and Yangtze River Delta Regions, Adv Atmos Sci, 26, 962-972, 10.1007/s00376-009-8001-2, 2009b.

Wei, X. L., Liu, Q., Lam, K. S., and Wang, T. J.: Impact of precursor levels and global warming on peak ozone concentration in the Pearl River Delta Region of China, Adv Atmos Sci, 29, 635-645, 10.1007/s00376-011-1167-4, 2012.

Xie, M., Wang, T.J., Jiang, F., Yang, X.Q.: Modeling of natural $NO_x$ and VOC emissions and their effects on tropospheric photochemistry in China, Environ. Sci. China, 28, 31-40, 2007.

Xie, M., Li, S., Jiang, F., and Wang, T. J.: Methane emissions from terrestrial plants over China and their effects on methane concentrations in lower troposphere, Chinese Sci Bull, 54, 304-310, 10.1007/s11434-008-0402-6, 2009.

Xie, M., Zhu, K. G., Wang, T. J., Yang, H. M., Zhuang, B. L., Li, S., Li, M. G., Zhu, X. S., and Ouyang, Y.: Application of photochemical indicators to evaluate ozone nonlinear chemistry and pollution control countermeasure in China, Atmos Environ, 99, 466-473, 10.1016/j.atmosenv.2014.10.013, 2014.

Xie, M., Liao, J., Wang, T., Zhu, K., Zhuang, B., Han, Y., Li, M., Li, S.: Modeling of the anthropogenic heat flux and its effect on regional meteorology and air quality over theYangtze River Delta region, China, Atmos. Chem. Phys., 16, 6071-6089, 10.5194/acp-16-6071-2016, 2016a.

Xie, M., Zhu, K. G., Wang, T. J., Chen, P. L., Han, Y., Li, S., Zhuang, B. L., and Shu, L.: Temporal characterization and regional contribution to O-3 and $NO_x$ at an urban and a suburban site in Nanjing, China, Sci Total Environ, 551, 533-545, 10.1016/j.scitotenv.2016.02.047, 2016b.

Yarwood, G., Rao, S., Yocke, M., Whitten G.: Updates to the Carbon Bond chemical mechanism: CB05., Final Report to the U.S. EPA, RT-0400675, 2005.

Zhang, X. Y., Zhang, P., Zhang, Y., Li, X. J., and Qiu, H.: The trend, seasonal cycle, and sources of tropospheric $NO_2$ over China during 1997-2006 based on satellite measurement, Sci China Ser D, 50, 1877-1884, 10.1007/s11430-007-0141-6, 2007.

Zhang, Y. H., Su, H., Zhong, L. J., Cheng, Y. F., Zeng, L. M., Wang, X. S., Xiang, Y. R., Wang, J. L., Gao, D. F., Shao, M., Fan, S. J., and Liu, S. C.: Regional ozone pollution and observation-based approach for analyzing ozone-precursor relationship during the PRIDE-PRD2004 campaign, Atmos Environ, 42, 6203-6218, 10.1016/j.atmosenv.2008.05.002, 2008.

Zhang, Q., Streets, D. G., Carmichael, G. R., He, K. B., Huo, H., Kannari, A., Klimont, Z., Park, I. S., Reddy, S., Fu, J. S., Chen, D., Duan, L., Lei, Y., Wang, L. T., and Yao, Z. L.: Asian emissions in 2006 for the NASA INTEX-B mission, Atmos Chem Phys, 9, 5131-5153, 2009.

Zhu, B., Kang, H. Q., Zhu, T., Su, J. F., Hou, X. W., and Gao, J. H.: Impact of Shanghai urban land surface forcing on downstream city ozone chemistry, J Geophys Res-Atmos, 120, 4340-4351, 10.1002/2014JD022859, 2015.